Graphene induced high-Q hybridized plasmonic whispering gallery mode microcavities

Mingming Jiang,[1,4] **Jitao Li,**[2,4] **Chunxiang Xu,**[2,5] **Shuangpeng Wang,**[1] **Chongxin Shan,**[1,*] **Bin Xuan,**[3] **Yongqiang Ning,**[1] **and Dezhen Shen**[1]

[1] *State key Laboratory of Luminescence and Applications, Changchun Institute of Optics, Fine Mechanics and Physics, Chinese Academy of Sciences, No.3888 Dongnanhu Road, Changchun, 130033, China*

[2] *State Key Laboratory of Bioelectronics, School of Biological Science and Medical Engineering, Southeast University, Nanjing 210096, China*

[3] *Key Laboratory of Optical System Advanced Manufacturing Technology, Changchun Institute of Optics, Fine Mechanics and Physics, Chinese Academy of Sciences, No.3888 Dongnanhu Road, Changchun, 130033, China*

[4] *These authors contributed equally to this work*

[5] *xcxseu@seu.edu.cn*

[*] *shancx@ciomp.ac.cn*

Abstract: A novel hybridized plasmonic whispering gallery mode (WGM) microcavities composed of graphene monolayer coated ZnO microrod with hexagonal cross section were proposed that operates in the ultraviolet region. π and $\pi+\sigma$ surface plasmon modes in graphene monolayer at 4.7 eV and 14.6 eV can be used to achieve the near field coupling interaction between surface plasmonic modes and the conventional WGM microcavity modes in the ultraviolet band. Significantly, the coupling, happened in the evanescent wave field excited along the interface between ZnO and graphene, can lead to distinct optical field confinement and lasing enhancement experimentally, so as well as WGM lasing characteristics, such as the higher cavity quality factor (Q), narrower linewidth, lasing intensities enhancement. The results could provide a platform to study hybridized plasmonic cavity dynamics, and also provides the building blocks to construct graphene based novel microcavity for high performance ultraviolet laser devices with potential application to optical signal processing, biological monitoring, and so on.

OCIS codes: (250.5403) Plasmonics; (140.0140) Lasers and laser optics; (140.3945) Microcavities.

References and links

1. K. J. Vahala, "Optical microcavities," Nature **424**(6950), 839–846 (2003).
2. J. Dai, C. X. Xu, and X. W. Sun, "ZnO-Microrod/p-GaN Heterostructured Whispering-Gallery-Mode Microlaser Diodes," Adv. Mater. **23**(35), 4115–4119 (2011).
3. B. Min, E. Ostby, V. Sorger, E. Ulin-Avila, L. Yang, X. Zhang and K. Vahala, "High-Q surface-plasmon-polariton whispering-gallery microcavity," Nature **457**(7228), 455–458 (2009).
4. L. He, S. K. Ozdemir and L. Yang, "Whispering gallery microcavity lasers," Laser Photonics Rev. **7**(1), 60–82 (2013).
5. C. X. Xu, J. Dai, G. P. Zhu, G. Y. Zhu, Y. Lin, J. T. Li, and Z. L. Shi, "Whispering-gallery mode lasing in ZnO microcavities," Laser Photonics Rev. **8**(4), 469–494 (2014).

#220257 - $15.00 USD Received 1 Aug 2014; revised 7 Sep 2014; accepted 8 Sep 2014; published 22 Sep 2014

6. R. Chen, B. Ling, X. W. Sun, H. D. Sun, "Room Temperature Excitonic Whispering Gallery Mode Lasing from High-Quality Hexagonal ZnO Microdisks," Adv. Mater. **23**, 2199–2204 (2011).
7. R. M. Ma, R. F Oulton, V. J Sorger, G. Bartal, and X. Zhang, "Room-temperature sub-diffraction-limited plasmon laser by total internal reflection," Nat. Mater. **10**, 110–113 (2011).
8. S. Christopoulos, G. von Högersthal, Höger Baldassarri, A. J. D.Grundy, P. G. Lagoudakis, A. V. Kavokin, J. J. Baumberg, G. Christmann, R. Butté, E. Feltin, J.-F. Carlin, and N. Grandjean, "Room-temperature polariton lasing in semiconductor microcavities," Phys. Rev. Lett. **98**, 126405 (2007).
9. M. H Huang, S. Mao, H. N. Feick, H. Q. Yan, Y. Y. Wu, Hannes Kind, E. Weber, R. Russo, and P. D. Yang, "Room-temperature ultraviolet nanowire nanolasers," Science **292**, 1897–1899 (2001).
10. D. Saxena, S. Mokkapati, P. Parkinson, N. Jiang, Q. Gao, H. H. Tan and C. Jagadish, "Optically pumped room-temperature GaAs nanowire lasers," Nat Photonics **7**, 963–968 (2013).
11. M. M. Jiang, B. Zhao, H. Y. Chen, D. X. Zhao, C. X. Shan and D. Z. Shen, "Plasmon-enhanced ultraviolet photoluminescence from the hybrid plasmonic Fabry–Perot microcavity of Ag/ZnO microwires," Nanoscale **6**, 1354–1361 (2014).
12. M. Ding, D. X. Zhao, B. Yao, S. L. E, Z. Guo, L. G. Zhang, and D. Z. Shen, "The ultraviolet laser from individual ZnO microwire with quadrate cross section," Opt. Express **20**, 13657–13662 (2012).
13. Da. J. Gargas, M. C. Moore, A. Ni, S. W. Chang, Z. Y. Zhang, S. L. Chuang and P. D. Yang, "Whispering gallery mode lasing from zinc oxide hexagonal nanodisks," ACS Nano **4**, 3270–3276 (2010).
14. G. Y. Zhu, C. X. Xu, L. S. Cai, J. T. Li, Ze. L. Shi, Y. Lin, G. F. Chen, T. Ding, Z. S. Tian, and J. Dai, "Lasing Behavior Modulation for ZnO Whispering-Gallery Microcavities," ACS Appl. Mater. Interfaces **4**, 6195–6201 (2012).
15. W. Jan, "Hexagonal dielectric resonators and microcrystal lasers," Phys. Rev. A **67**, 023807 (2003).
16. G. Marius and D. Christof P, "Whispering gallery modes in deformed hexagonal resonators," Phys. Status Solidi B **249**, 871–879 (2012).
17. H. Kudo, R. Suzuki, and T. Tanabe, "Whispering gallery modes in hexagonal microcavities," Phys. Rev. A **88**, 023807 (2013).
18. T. Nobis and M. Grundmann, "Low-order optical whispering-gallery modes in hexagonal nanocavities," Phys. Rev. A **72**, 063806 (2005).
19. S. Takao, W. Ralph, F. Alfred, C. Massimo, C. Roberto, and A. Yasuhiko, "Room temperature lasing at blue wavelengths in gallium nitride microcavities," Science **285**, 1905–1906 (1999).
20. Y. F. Xiao, C. L. Zou, B. B. Li, Y. Li, C. H. Dong, Z. F. Han, Q. H. Gong, "High-Q Exterior Whispering-Gallery Modes in a Metal-Coated Microresonator," Phys. Rev. Lett. **105**, 153902 (2010).
21. Y. L. Chen, C. L. Zou, Y. W. Hu and Q. H. Gong, "High-Q plasmonic and dielectric modes in a metal-coated whispering-gallery microcavity," Phys. Rev. A **87**, 023824 (2013).
22. K. Ding and C. Z. Ning, "Metallic subwavelength-cavity semiconductor nanolasers," Light: Sci. Appl. **1**, e20 (2012).
23. Y. H. Su, Y. F. Ke, S. L. Cai and Q. Y. Yao, "Surface plasmon resonance of layer-by-layer gold nanoparticles induced photoelectric current in environmentally-friendly plasmon-sensitized solar cell," Light: Sci. Appl. **1**, e14(2012).
24. R. F. Oulton, V. J. Sorger, T. Zentgraf, R. M. Ma, C. Gladden, L. Dai, G. Bartal and X. Zhang, "Plasmon lasers at deep subwavelength scale," Nature **461**, 629–632 (2009).
25. J. M. Yao, A. P. Le, S. K. Gray, J. S. Moore, J. A. Rogers and R. G. Nuzzo, "Functional nanostructured plasmonic materials," Adv. Mater. **22**, 1102–1110 (2010).
26. P. R. West, S. Ishii, G. V. Naik, N. K. Emani, V. M. Shalaev and A. Boltasseva, "Searching for better plasmonic materials," Laser Photonics Rev. **4**, 795–808 (2010).
27. V. G. Kravets, A. N. Grigorenko, R. R. Nair, P. Blake, S. Anissimova, K. S. Novoselov, and A. K. Geim, "Spectroscopic ellipsometry of graphene and an exciton-shifted van Hove peak in absorption," Phys. Rev. B **81**, 155413 (2010).
28. A. N. Grigorenko, M. Polini and K. S. Novoselov, "Graphene plasmonics," Nature Photonics **6**, 749–758 (2012).
29. R. R. Nair, P. Blake, A. N. Grigorenko, K. S. Novoselov, T. J. Booth, T. Stauber, N. M. R. Peres, and A. K. Geim, "Fine structure constant defines visual transparency of graphene," Science **320**, 1308 (2008).
30. F. H. L. Koppens, D. E. Chang, and F. Javier Garcia de Abajo,, "Graphene plasmonics: a platform for strong light–matter interactions," Nano Lett. **11**, 3370–3377 (2011).
31. W. L. Gao, J. Shu, C. Y. Qiu, and Q. F. Xu, "Excitation of plasmonic waves in graphene by guided-mode resonances," ACS Nano **6**, 7806–7813 (2012).
32. R. Chanaka, R. I. D, Premaratne, Malin, "Spaser Made of Graphene and Carbon Nanotubes," ACS Nano **8**, 2431–2438 (2014).
33. S. W. Hwang, D. H. Shin, C. Oh Kim, S. H. Hong, M. C. Kim, J. Kim, K. Y. Lim, S. Kim, S. Choi, K. J. Ahn, G. Kim, S. H. Sim, and B. H. Hong, "Plasmon-enhanced ultraviolet photoluminescence from hybrid structures of graphene/ZnO films," Phys. Rev. Lett. **105**, 127403 (2010).
34. M. Jablan, H. Buljan, M. Soljačić, "Plasmonics in graphene at infrared frequencies," Phys. Rev. B **80**, 245435 (2009).

#220257 - $15.00 USD Received 1 Aug 2014; revised 7 Sep 2014; accepted 8 Sep 2014; published 22 Sep 2014

35. Y. Y. Lai, Y. P. Lan and T. C. Lu, "Strong light–matter interaction in ZnO microcavities," Light: Sci. Appl. **2**, e76 (2013).
36. L. Yang, J. Deslippe, C. H. Park, M. L. Cohen, and S. G. Louie, "Excitonic Effects on the Optical Response of Graphene and Bilayer Graphene," Phys. Rev. Lett. **103**, 186802 (2009).
37. N. I. Zheludev, S. L. Prosvirnin, N. Papasimakis and V. A. Fedotov, "Lasing spaser," Nat Photonics **2**, 351–354 (2008).
38. O. L. Berman, R. Ya. Kezerashvili, and Y. E. Lozovik, "Graphene nanoribbon based spaser," Phys. Rev. B **88**, 235424 (2013).
39. M. L. Gorodetsky, A. A. Savchenkov, and V. S. Ilchenko, "Ultimate Q of optical microsphere resonators," Opt Lett. **21**, 453–455 (1996).
40. T. Nobis, E. M. Kaidashev, A. Rahm, M. Lorenz, and M. Grundmann, "Whispering gallery modes in nanosized dielectric resonators with hexagonal cross section," Phys. Rev. Lett. **93**, 103903 (2004).
41. T. Eberlein, U. Bangert, R. R. Nair, R. Jones, M. Gass, A. L. Bleloch, K. S. Novoselov, A. Geim, and P. R. Briddon, "Plasmon spectroscopy of free-standing graphene films," Phys. Rev. B **77**, 233406(2008).
42. P. E. Trevisanutto, C. Giorgetti, L. Reining, M. Ladisa, and V. Olevano, "Ab Initio GW Many-Body Effects in Graphene," Phys. Rev. Lett. **101**, 226405 (2008).
43. S. Das Sarma and E. H. Hwang, "Collective Modes of the Massless Dirac Plasma," Phys. Rev. Lett. **102**, 206412 (2009).
44. Y. Liu and R. F. Willis, "Plasmon-phonon strongly coupled mode in epitaxial graphene," Phys. Rev. B **81**, 081406(R) (2010).
45. Y. Liu, R. F. Willis, K. V. Emtsev, and Th. Seyller, "Plasmon dispersion and damping in electrically isolated two-dimensional charge sheets," Phys. Rev. B **78**, 201403(R)(2008).
46. A. Vakil and N. Engheta, "Transformation optics using graphene," Science, **332**, 1291–1294 (2011).
47. J. T. Li, C. X. Xu, H. Y. Nan, M. M. Jiang, G. Y. Gao, Y. Lin, J. Dai, G. Y. Zhu, Z. H. Ni, S. F. Wang, and Y. Li, "Graphene Surface Plasmon Induced Optical Field Confinement and Lasing Enhancement in ZnO Whispering-Gallery Microcavity," ACS Appl. Mater. Interfaces **6**, 10469–10475 (2014).
48. V. Apalkov, M. I Stockman, "Proposed graphene nanospaser," Light: Sci. Appl. **3**, e191 (2014).
49. I. Santoso, R. S. Singh, P. K. Gogoi, T. C. Asmara, D. Wei, W. Chen, A. T. S. Wee, V. M. Pereira, and A. Rusydi, "Tunable optical absorption and interactions in graphene via oxygen plasma," Phys. Rev. B **89**, 075134 (2014).
50. C. H. Gan, H. S. Chu, and E. P. Li, "Synthesis of highly confined surface plasmon modes with doped graphene sheets in the midinfrared and terahertz frequencies,"Phys. Rev. B **85**, 125431 (2012).
51. G. W. Hanson, "Dyadic Greens functions and guided surface waves for a surface conductivity model of graphene," J App. Phys. **103**, 064302 (2008).
52. C. H. Gan, "Analysis of surface plasmon excitation at terahertz frequencies with highly doped graphene sheets via attenuated total reflection," App. Phys. Lett. **101**, 111609 (2012).
53. L. B. Yu, E. Barakat, T. Sfez, L. Hvozdara, J. Di Francesco and H. P. Herzig, "Manipulating Bloch surface waves in 2D: a platform concept-based flat lens," Light: Sci. Appl. **3**, e124 (2014).
54. W. L. Barnes, Al. Dereux and T. W. Ebbesen, "Surface plasmon subwavelength optics," Nature **424**, 824 (2003).
55. J. Zhao, X. H. Liu, W. B. Qiu, Y. H. Ma, Y. X. Huang, J. X. Wang, K Qiang, and J. Q. Pan, "Surface-plasmon-polariton whispering-gallery mode analysis of the graphene monolayer coated InGaAs nanowire cavity," Opt. Express **22**, 5754 (2014).
56. M. P. Nezhad, A. Simic, O. Bondarenko, B. Slutsky, A. Mizrahi, L. Feng, V. Lomakin and Y. Fainman, "Room-temperature subwavelength metallo-dielectric lasers," Nat. Photonics **4**, 395–399 (2010).
57. R. M. Cole, Y. Sugawara, and J. J. Baumberg, "Easily Coupled Whispering Gallery Plasmons in Dielectric Nanospheres Embedded in Gold Films," Phys. Rev. Lett. **97**, 137401 (2006).

1. Introduction

Ultrahigh-Q factor microresonators have a lot of applications in the photonics domain ranging from low-threshold nonlinear optics to integrated optical sensors as well [1–8]. Up till the present moment, the major challenge for designation of these optical cavities is ensuring control and reproducibility of waveguide-to-resonator coupling and resonator dimensions, as well as spectral shape and filter roll-off characteristics of these devices. Blue and ultraviolet lasers are attracting much interest due to the wide range of foreseen applications (display, optical data storage, biomedical). GaN, ZnO based semiconductor materials and various kinds of optical resonators have been investigated, such as Fabry-Perot (F-P) modes in planar microcavities and in nanowires [9–12], whispering gallery mode (WGM) cavities in microwires and microdisks, cavities in photonic crystal membranes, as well as random lasing in ZnO powders and waveguides [13–15]. While possessing natural resonant cavities, ZnO, GaN nanowires and

#220257 - $15.00 USD Received 1 Aug 2014; revised 7 Sep 2014; accepted 8 Sep 2014; published 22 Sep 2014

microwires provide an ideal platform to investigate the optical resonators. Recently, obvious WGM lasing based on ZnO microrod with hexagonal cross section has been realized [16–18], as well as WGM lasing in GaN [19]. However, pristine optical cavity resonators exist inevitable loss, such as radiation loss, mirror loss and waveguide loss.

Surface plasmon polaritons (SPPs) are electron density waves excited at the interfaces between metals and dielectric materials. Owing to their highly localized electromagnetic fields, SPPs may be used for the transport and manipulation of photons on subwavelength scales. Plasmonic resonant cavities represent an application that could exploit this field compression to create ultrasmall-mode-volume devices. Metal-coated WGM microcavities have been exploited and found that hybrid microcavities can support plasmonic modes, which leads to a stronger confinement and lower radiation losses [3, 20, 21]. In addition, high-Q surface-plasmon-polariton WGM microcavity reported by Bumki Min has greatly inspired researchers' interests [20–24]. Experimentally, the realization of achievable high-Q factors for plasmonic resonant structures is a very serious challenge. Metal loss is still an insurmountable difficulty towards the applications of plasmonics on the nano/micro-scale. Compared with metal optical materials, such as silver and gold, graphene is another material that has generated excitement in the research community due to its unique band structure and high carrier mobility [25–29]. Extreme field confinement, device tunability and patterning, and low losses that emerge from the remarkable structure of graphene and current experimental capabilities for fabrication have been realized [30]. Highly confined plasmonic waves in graphene monolayers have been achieved by means of guided-wave resonance [31, 32]. These advances are expected to both remove a number of obstacles facing traditional metal plasmonics and facilitate new possibilities for manipulating light-matter interactions at the nanoscale down to the single-SPP level [33]. When applied to gain medium, such as GaN, ZnO, graphene could offer ideal platform for cavity quantum electrodynamics [30, 34, 35]. Resonant excitonic effects in graphene and bilayer graphene result in significant changes in the optical absorption spectrum in the energy regime near a van Hove singularity as compared to the independent-particle picture [27, 32, 36–38].

However, the application of graphene plasmons in wide bandgap semiconductor materials based microcavities operated in the ultraviolet region have yet to be resolved. In this letter, a hybridized plasmonic WGM microcavity consisting of graphene monolayer covered ZnO microrod with hexagonal cross section was proposed. ZnO hexagonal microrod can be treated as intrinsic WGM type microcavity, whilst as the gain medium. Graphene monolayer supports the surface plasmon wave field, which provides a platform to study the coupling interaction between graphene surface plasmonic modes and conventional WGM modes. Take the corresponding plasmonic microcavity dynamic into account, WGM lasing characteristics on the basis of graphene coated ZnO hexagonal microrod were carried out experimentally.

2. Results and discussion

2.1. Whispering gallery mode microresonator based on hexagonal microrod

For the hexagonal WGM resonance, the relationship between the resonance wavelength λ and corresponding mode serial number N can be deduced as [15, 40]:

$$\frac{1}{\lambda} = \frac{2}{3\sqrt{3}nD}\left[N + \frac{6}{\pi}\tan^{-1}(\beta\sqrt{3n^2-4})\right] \tag{1}$$

where D is the circum circle diameter of hexagonal microcavity, β denotes n $(1/n)$ for **TE** (**TM**) polarization and n is the relative refractive index of ZnO microrod to the outside medium.

#220257 - $15.00 USD Received 1 Aug 2014; revised 7 Sep 2014; accepted 8 Sep 2014; published 22 Sep 2014

The corresponding Q-factor of WGM microcavity has been calculated as following [15, 40]:

$$Q = \frac{m\pi nDR^{m/4}}{2\lambda(1-R^{m/2})} \sin\left(\frac{2\pi}{m}\right). \tag{2}$$

In an m-faceted polygonal cavity, the Q-factor is given by where m is the number of facets, n is the refractive index of the dielectric material, D is the diameter of the circle circumscribing the polygon, and R is the reflectivity of the facet mirrors. The reflectivity, R, has been reported as 87% for WGM; these reflectivities are quite reasonable for WGM or quasi-WGM resonance [2, 4, 5]. Previous reportes on high Q-factor suggest that the observed lasing emissions resulted from WGM resonance in a hexagonal dielectric resonator rather than from the F-P mode [2, 4–6, 13, 14]. A much smaller reflectivity and Q-factor would be expected for the F-P mode, which is not consistent with the experimental results. The WGM lasing behaviors and lasing characteristics are relevant to configurations of WGM microcavities, as well as the effective mode index [14]. Therefore, the modulation of the effective mode index of hybrid optical microcavities can be used to modify the lasing behaviors, lasing mode numbers, optical field distribution and the lasing Q-factor.

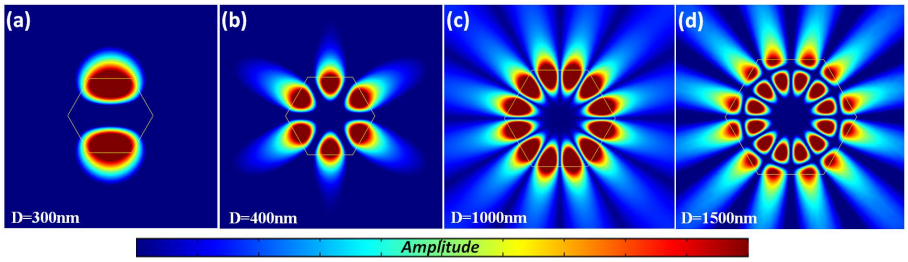

Fig. 1. Simulation of near field $\mathbf{E}(x,y)$ patterns of the hexagonal cross section of ZnO microrod resonator with different diameter shown in the inset. The corresponding resonant wavelength around 390 nm.

The total intrinsic loss of a whispering-gallery resonator is given as [39]: $1/Q_{tot} = 1/Q_r + 1/Q_m + 1/Q_s$, where Q_r^{-1} is the radiative loss, Q_m^{-1} is the modal loss related to the material absorption and Q_s^{-1} is the loss contribution accounting for both the surface scattering and surface absorption. In particular, the quality factor Q_{tot}, is dependent heavily on the material and modal loss, and denoted as $Q_m = \lambda_r(\Gamma\alpha\Lambda r_{eff})^{-1}$, where α is the absorption coefficient of microcavity materials, Λ is the free-spectral range of the cavity modes, λ_r is the resonant wavelength, r_{eff} is the effective radius of WGM microcavity and Γ is the confinement factor of the mode. Therefore, the material and modal loss rely mainly on the r_{eff}. To further demonstrate the loss mechanism related to different diameter, the two-dimensional (2D) time domain and frequency domain finite element method (FDTD) have been carried out. Near field $\mathbf{E}(x,y)$ patterns of the hexagonal cross section of ZnO microrod resonator has been demonstrated in Fig. 1 with different diameters. The corresponding resonant wavelength was set as 390 nm. By taking the Q_s^{-1} into account, the sidewall effects in terms of modes' interaction with the resonators external rim by scattering due to roughness, and absorption by specimen on the surface, can also be referred to the Fig. 1. For a small size of microwire ($D \ll L$), the cavity diameter is much smaller and the reflection coefficient of mirror surfaces is small, so the waveguide loss can be neglected. But for a large diameter of microwires, in which the waveguide loss should be large and considered in the ZnO microwire WGM lasers [2, 4, 5, 11, 12, 14, 47]. According to the Fig. 1(d), D = 1500 nm, the microcavity loss and the WGM resonance characteristic can be co-existence.

#220257 - $15.00 USD Received 1 Aug 2014; revised 7 Sep 2014; accepted 8 Sep 2014; published 22 Sep 2014

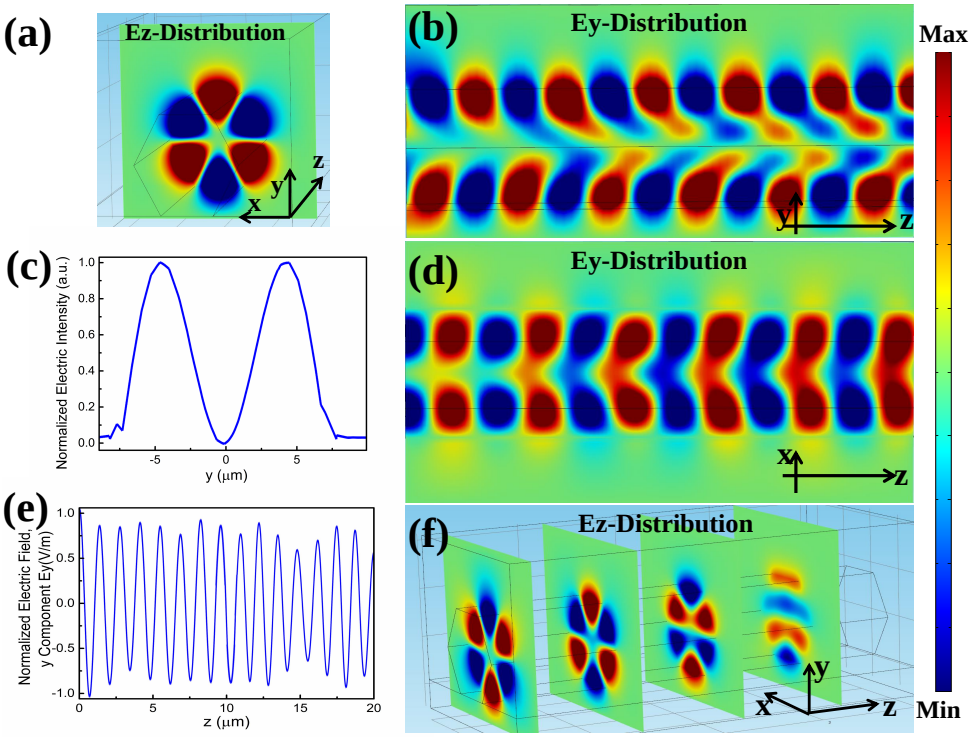

Fig. 2. Calculated electric field intensity distribution of a bare ZnO microrod placed on substrate: (a) z component of electrical field distribution along x-y-plane, which a slice of the bare microrod, could demonstrate the WGM mode characteristics; (b) and (d) show y component of electrical field distribution along y-z-plane, x-z-plane, respectively; (c) indicates the WGM modes of a bare ZnO microrod with hexagonal cross section; (e) displays y component of electrical field distribution along y-z-plane, which can reveal the photons escaped from the WGM microcavity transmission process along the axis of microrod; (f) z component of electrical field distribution along x-y-plane with four slices of the bare microrod. Corresponding parameters $n_{ZnO} = 2.5$, $n_{SiO_2} = 1.5$, $n_{air} = 1$, and the diameter of ZnO microrod $D = 10\ \mu m$, with corresponding calculated wavelength λ_0 = 390 nm. The centre of the microrod defines the origin ($x = y = 0$.)

Because of the inevitable waveguide loss of ZnO microrod, part of excited photons of ZnO microrod would propagate along the axis of microd under optical pumping. Therefore, a model of a bare ZnO microrod placed on SiO_2 substrate shown in Fig. 2 was built, this kind of model can be used to reveal the oscillation transmission process of the photons, which escaped from the WGM microcavity by means of 3D finite-difference time-domain (FDTD) methods. As a matter of fact, the waveguide loss of ZnO microrod is much more serious [5, 12, 14]. Figure 2(a) shows z component of electrical field distribution E_z along x-y-plane, which a slice of the bare microrod. The E_z-distribution could display unambiguous WGM modes characteristics. Figures 2(b) and 2(d) show y component of electrical field distribution along y-z-plane, x-z-plane, respectively. The existence of waveguide loss would result in part of photons escaped from WGM modes and then could propagate along the axis of microrod. Obvious attenuation processes of the waveguide loss and mirror loss have been demonstrated in Figs. 2(b) and 2(d). The attenuation process of photons along the z-axis can also be obtained, and shown in Fig. 2(e). Figure 2(c) has indicated the optical field energy distribute along the $x-y$ plane of the cross

#220257 - $15.00 USD Received 1 Aug 2014; revised 7 Sep 2014; accepted 8 Sep 2014; published 22 Sep 2014

section of the optical WGM microcavity. Figure 2(f) demonstrates z component of electrical field distribution along x-y-plane with four slices of the bare microrod. Obviously, the photons escaped from the WGM microcaity propagate along the axis of ZnO microrod gradually losing its WGM lasing characteristics.

2.2. *Graphene surface plasmon modes in ultraviolet wavelength region*

Graphene, a strictly two-dimensional material that can exhibit exceptionally high crystal and electronic quality, and has already revealed a cornucopia of new physics and potential applications [25, 26, 28–30, 32, 36, 42, 46]. Because of the peculiar electronic structure of graphene, it could be interesting to study the photoexcitation with ultrashort coherent pulses in the ultraviolet (UV) spectral region. Plasmon spectroscopy of the thinnest possible membrane, a single layer of carbon atoms: graphene, has been carried out in conjunction with *ab initio* calculations of the low loss function. π and $\pi+\sigma$-surface plasmon modes in free-standing single sheets at 4.7 and 14.6 eV has been observed [41]. To confirm the plasmon spectroscopy of free standing graphene monolayer, an *ab initio* numerical many-body GW calculation of the band plot in freestanding graphene has been carried out. Close to the Dirac point the linear dispersion is modified by the presence of a kink, as observed by angle-resolved photoemission spectroscopy. The kink is due to low-energy $\pi \rightarrow \pi^*$ single-particle excitations and to the π plasmon [33, 42, 43]. At the K point of the reciprocal space, the electronic band structure displays a vanishing density of states (DOS) and a vanishing energy gap between the valence and conduction bands that shows, for a single layer, an identical linear k dispersion of the two p bands. Therefore, surface plasmon of graphene monolayer can be happened in the ultraviolet band.

Let us model the graphene monolayer as a surface conducting sheet. In the ultraviolet band, $\pi+\sigma$ plasmon scattering dominates in graphene monolayer, and its plasmon energy can be taken the form [33, 44, 45]:

$$\omega(q) = \Big[\frac{4\pi n_e e^2}{m^*(1+\varepsilon_{ZnO})}q + \frac{3}{4}\upsilon_F^2 q^2 + \cdots\Big]^{1/2}, \tag{3}$$

where n_e is the number of electrons in a unit area, ε_0 is the vacuum permittivity, ε_{ZnO} is the background dielectric constant, m^* is the effective mass of the graphene electrons, and υ_F is the Fermi velocity, and q is the in-plane wave number, which can be used to regard q-dependent energy dispersion relation of graphene plasmon $\omega(q)$. Alternatively, graphene, not only possesses intrinsic plasmons that are tunable and adjustable, but a combination of graphene with micro/nanostructures can motivate a variety of exciting applications for conventional plasmonics. Proper choice of conductivity spatial patterns across the graphene layers could provide exciting possibilities for tailoring, manipulating, and scattering SPP wave signals across the graphene layers. The surface plasmon wave can be engineered to reflect and refract on this sheet of graphene by varying the injection of different wavelengths and different field energy [46].

Let us define the effective mode index of the supported plasmon mode as $n_{eff} = \beta/k_0$, where $k_0 = 2\pi/\lambda$, and λ is the free space wavelength. In the local limit $\omega \gg \tau^{-1}$, the condition $\beta\upsilon_F \leq \omega$ can result in the translation into the formation of $n_{eff} \leq c/\upsilon_F$. To analysis the surface plasmon excitation shown in Fig. 2, the model can be simplified as air/graphene/ZnO. Each graphene monolayer can be regarded as a surface conducting sheet, and its conductivity σ takes on a Drude-like form of $\sigma \approx ie^2\mu/\big[\pi\hbar^2(\omega+i\tau^{-1})\big]$, where $\mu = \hbar\upsilon_F\sqrt{n_e\pi}$, υ_F is the Fermi velocity, n_e is the carrier density, $\omega = k_0 c$ is the angular frequency with c the speed of light in vacuum, τ is a phenomenological electron relaxation time, and the local limit $\omega \gg \tau^{-1}$ [50–53]. For a guided wave with wave number β propagating along the x axis, the plasmon dispersion

#220257 - $15.00 USD Received 1 Aug 2014; revised 7 Sep 2014; accepted 8 Sep 2014; published 22 Sep 2014

relation can be reduced into the form:

$$\frac{\varepsilon_{air}}{k_{x(air)}} + \frac{\varepsilon_{ZnO}}{k_{x(ZnO)}} + \frac{i\sigma}{\omega\varepsilon_0} = 0, \tag{4}$$

where $k_{x(ZnO)/ZnO} = \sqrt{\varepsilon_{air/ZnO}}k_0$. Therefore, the above dispersion relation yields the approximations

$$\beta_{sp}(\omega) = \frac{\sqrt{\pi}\varepsilon_0\hbar c}{e^2 \upsilon_F \sqrt{n_e}}\left(\varepsilon_{air} + \varepsilon_{ZnO}\right)\left(\omega^2 + i\omega\tau^{-1}\right) \tag{5}$$

This dispersion relation bears a striking resemblance with that for the SPs at a metal-dielectric interface. If either one of the dielectric media is a metal, then it is clear that the SP mode is almost identical to that for the metal-dielectric interface [50–52]. The surface plasmon wavelength λ_{sp} can be obtained $\lambda_{sp} = 2\pi/(\mathbf{Re}(\beta_{sp}(\omega)))$. The remarkable degree of confinement provided by the graphene is clear from the ratio of SP to free-space-light wavelengths

$$\frac{\lambda_{sp}}{\lambda_0} = \frac{e^2 \upsilon_F \sqrt{n_e}}{\sqrt{\pi}\varepsilon_0\hbar c^2(\varepsilon_{air} + \varepsilon_{ZnO})}\frac{1}{\omega + i\tau^{-1}}. \tag{6}$$

In addition, the out-of-plane wave vector $\sim i\beta_{sp}$ indicates an equally tight confinement to dimensions $\sim \lambda_{sp}/2\pi$ in the transverse direction x [30, 50–53]. Strong SPPs confinement can lead to significant lateral enhancement of the electromagnetic field, well beyond what is found in transparent dielectric materials, this results in enhancement of field energy. Notwithstanding, the collective oscillation of the electrons in graphene monolayer have the abilities to strongly confine light at the subwavelength scale,

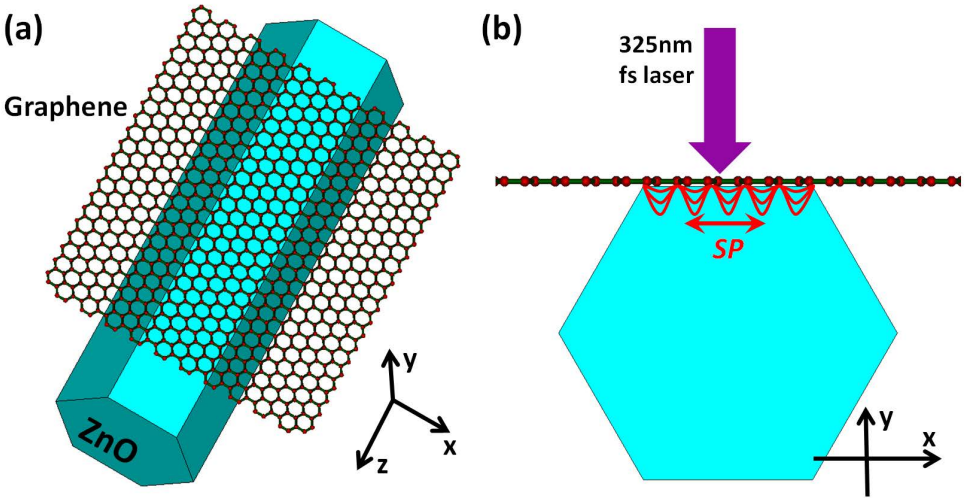

Fig. 3. (a) schematic diagram of graphene monolayer coated ZnO hexagonal microrod; (b) Excitation of surface plasmons along the interface between graphene and ZnO, the hybrid structures can be treated as air/graphene/ZnO, evanescent wave field excited along the interface confined within ZnO, which provides a platform to achieve the coupling between surface plasmonic mode and the conventional WGM microcavity mode.

In consequence, a hybridized plasmonic WGM microstructure was proposed consisting of a ZnO hexagonal microrod coated by a graphene monolayer. This kind of hybridized plasmonic WGM microcavity can achieve the coupling between conventional optical cavity modes with

#220257 - $15.00 USD Received 1 Aug 2014; revised 7 Sep 2014; accepted 8 Sep 2014; published 22 Sep 2014

surface plasmonic modes. Schematic diagram of the hybridized plasmonic WGM microcavity was represented in Fig. 3(a). The length of microbelt goes along the z axis. A crossover region exists along the interface between ZnO and graphene. The absorption, can induce collective oscillation of the two-dimensional electron gas, and this kind of collective oscillation can lead to localized surface plasmons excited along the interface. The excited evanescent wave field of graphene would be confined in crossover region, depicted in Fig. 3(b), indicating that the evanescent wave field supported by graphene monolayer is strongly localized at subwavelength scale [47, 48]. The crossover region is dependent on the real part of the effective mode index and ZnO. This anticrossing appears because of the coupling between the cavity mode and the surface plasmonic modes supported by the air-semiconductor-metal multilayer. Therefore, the crossover region can provide a platform to achieve the coupling between the surface plasmonic modes and conventional WGM resonant modes. In addition, the crossover region relies on the depth of the evanescent wave field penetrating into ZnO microbelt. More detail information on the theoretical calculation and simulation can be referred to the next section below.

2.3. Hybridized plasmonic whispering gallery mode microcavity

The hybridized plasmonic WGM microcavities consisting of graphene monolayer coated ZnO microrod with hexagonal cross section will be turned attention on to investigate the localized plasmon effect in WGM microcavities [32,37,47,54]. Strong SPPs confinement in such system can lead to significant lateral enhancement of the electromagnetic field, well beyond what is found in transparent dielectric materials, this results in enhancement of spontaneous emission [32, 38, 48]. How to reduce the mirror loss of ZnO hexagonal microrod, which treated as the intrinsic WGM optical microcavity, is the key factor to prevent energy leakage outward. An approach is to modulate the localized field distribution of the mirrors. The hexagonal cross section of ZnO microrod coated by graphene, which a slice of the model shown in Fig. 3 was extracted, and then calculated and simulated by means of COMSOL Multiphysics software.

As mentioned above, one of the challenges of using a WGM cavity as the basis for creating a hybridized plasmonic WGM lasing is achieving efficient energy transfer from the evanescent field of the cavity to the graphene monolayer. In this section, the hybridized surface plasmonic modes and coupling between SPP modes and the conventional optical WGM microcavities modes were studied. The proposed models have been grouped into two categories: a bare ZnO hexagonal microrod placed on the SiO_2 substrate; a ZnO hexagonal microrod placed on the SiO_2 substrate coated by a single graphene monolayer, and with two single graphene monolayer coated on the upper and down surface of ZnO microrod, respectively. The effective microcavity mode index n_{hyb}, denoted as $n_{hyb} = \beta(\omega)/k_0$, can be calculated from the model demonstrated in Fig. 3. The effective microcavity mode index n_{hyb} is important because it can be used to determine the eigenmodes of hybridized plasmonic WGM microcavities. The eigenmodes of the hybridized plasmonic WGM microcavity can be classified into three distinctive categories in terms of the cavity mode dispersion: the conventional optical WGM modes, surface plasmonic modes at the graphene/ZnO interface, and the hybridized plasmonic WGM modes between the conventional optical WGM modes and surface plasmonic modes. ZnO microrod with hexagonal cross section possesses natural WGM cavity mode characteristics shown in Fig. 4(a), corresponding to effective mode refractive index n_{hyb} = 2.4903 [15–18]. When coated by a graphene monolayer on the upper surface of ZnO microrod, the SPPs supported by graphene monolayer has been demonstrated in Fig. 4(b), which displays the hybrid plasmonic WGM mode composed of the SPP mode and dielectric mode with corresponding effective mode refractive index n_{hyb} = 2.498. Figure 4(c) displays unmixed SPPs mode supported by graphene, corresponding effective mode refractive index $n_{hyb} = 2.63$. Figure 4(b) illustrates the impact of the near-field coupling between ZnO microrod and graphene monolayer. The evanescent wave

#220257 - $15.00 USD Received 1 Aug 2014; revised 7 Sep 2014; accepted 8 Sep 2014; published 22 Sep 2014

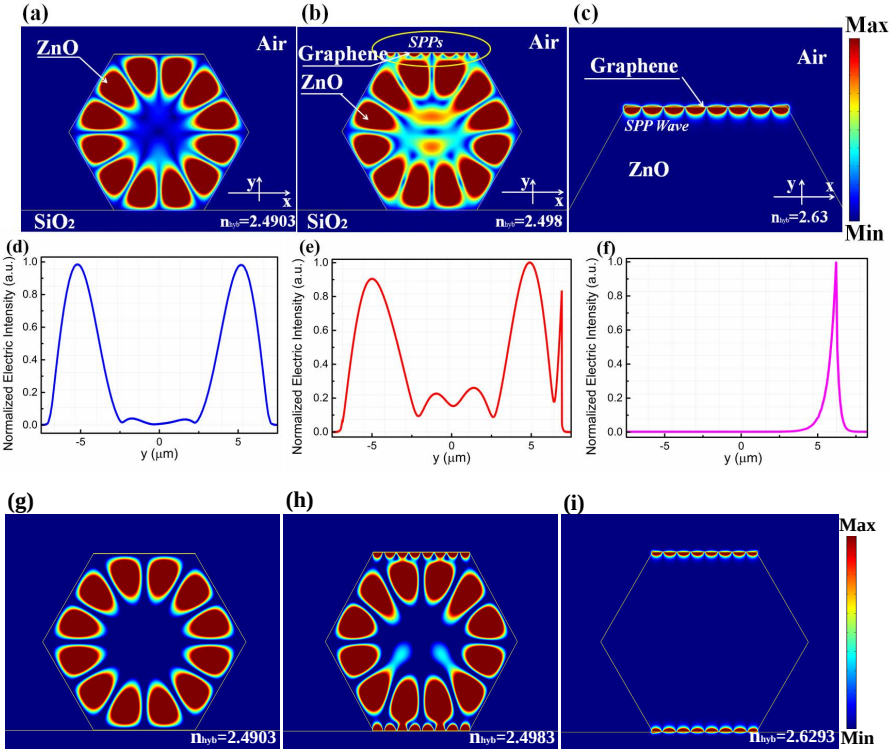

Fig. 4. Hybrid plasmonic WGM microcavities: (a) displays the WGM modes of a bare ZnO microrod with hexagonal cross section, corresponding effective mode refractive index $n_{hyb} = 2.4903$; (b) displays the hybrid plasmonic WGM mode composed of the SPP mode and dielectric mode. On the basis of the upper surface of ZnO microrod covered by graphene monolayer, guided SPPs would be confined within the contact area between graphene and ZnO, corresponding effective mode refractive index $n_{hyb} = 2.498$; (c) displays unmixed SPPs mode supported by graphene, corresponding effective mode refractive index $n_{hyb} = 2.63$; (d)-(f) plot the normalized electric field intensities of optical WGM mode, hybridized plasmonic WGM mode and unmixed SPPs mode along the y axis, respectively; (g)-(i) demonstrate the conventional optical WGM microcavity mode with $n_{hyb} = 2.4903$, the hybrid plasmonic WGM mode composed of the SPP mode and dielectric mode with $n_{hyb} = 2.4983$ and unmixed SPPs mode supported by graphene monolayer with $n_{hyb} = 2.6293$, respectively. The incident calculated wavelength λ_0 = 390 nm, relative index of refraction of graphene monolayer $\varepsilon_{graphene} = 5.28 + 7.78i$ [27, 36, 49] with the thickness of graphene monolayer set 0.5 nm.

generated from graphene monolayer can infiltrate into ZnO microrod. Obviously, the original WGM cavity modes have been affected by the evanescent field distributed in the hexagonal cross section. In addition, Figure 4(b) demonstrates the superposition excitation light field and the field of graphene monolayer SPPs mode. Their energies are stored in the form of the collective oscillation of electrons in graphene monolayer and an evanescent wave penetrating into ZnO microrod. Graphene can induce more energy distributed along the interface between graphene and ZnO.

In order to more clearly illuminate that graphene plasmon can improve electric energy intensities distribution on the surface of ZnO hexagonal microrod, normalized electric field inten-

#220257 - $15.00 USD Received 1 Aug 2014; revised 7 Sep 2014; accepted 8 Sep 2014; published 22 Sep 2014

sities of optical WGM modes, hybridized plasmonic WGM modes and unmixed SPPs modes along the y axis have been plotted respectively, and have been demonstrated in Figs 4(d) - 4(f). Figures 4(e) and 5(b) demonstrate that graphene monolayer can achieve the optical field confined around the interface. Significantly, the interactions between graphene and conventional WGM microcavity of ZnO hexagonal microrod could be enhanced and supports fundamentally new capabilities to enhance the lasing. Figure 4(e) reveals that a clear overlap occurs where two energy eigenvalues come near to cross but then repel each other, similar to the strong interaction between a microcavity resonance modes and graphene surface plasmon modes. This is the signature of a strong coupling between the fundamental WGM mode and surface plasmonic modes. All these provide important evidence for optimizing the threshold condition of WGM lasing for ZnO hexagonal microrods. From another perspective, ZnO hexagonal microrod, acted as gain medium and the laser resonator, is not conducive to the stability of the cavity. Existence of evanescent fields could adjustable be able to compensate the photon energy losses, increasing the laser threshold of microcavity lasing.

To further investigate the surface plasmonic effect of graphene monolayer, the model of two single graphene monolayers coated on the upper and down surface of ZnO microrod respectively was taken into account. Figure 4(g) – 4(i) demonstrate the conventional optical WGM microcavity mode with $n_{hyb} = 2.4903$, the hybrid plasmonic WGM mode composed of the SPP mode and dielectric mode with $n_{hyb} = 2.4983$ and unmixed SPPs mode supported by graphene monolayer with $n_{hyb} = 2.6293$, respectively. Obviously, the more contacts of graphene monolayer with the surfaces of ZnO microrod, the coupling interaction between graphene and ZnO microrod will be stronger. These results are corresponding to the model shown in Fig. 1. In addition, the improvement of energy distribution shown in Figs. 4(b), 4(e), 4(h) also confirmed that more photons will be confined to the interface between ZnO and graphene, which indicated that confinement performance of the light field got obvious improvement.

To achieve the maximal spasing efficiency, the hybridized plasmonic WGM modes of spaser could be realized by means of resonantly coupling to the ZnO excitons by matching the graphene monolayer SPP mode energy with the energy of ZnO excitons [32, 38]. Focusing on the field confinement effects of graphene, we here restrict our calculations to resonant excitation condition based on graphene coated WGM microcavity, the electromagnetic scattering induced on the basis of external electromagnetic field projected into bound atoms of graphene was taken into account. The harmonic oscillator as a model was used as the bound electrons within the graphene. The natural frequency of the harmonic oscillator was treated as ω_0, under the action of the incident wave field $\mathbf{E}_0 e^{-i\omega t}$, a dynamic evolution process is constructed for the generalized frequency dependent harmonic oscillator by employing the solution to the corresponding classical equations of motion:

$$\ddot{\mathbf{x}} + \gamma\dot{\mathbf{x}} + \omega_0^2\mathbf{x} = \frac{e}{m}\mathbf{E}_0 e^{-i\omega t},\ \gamma = \frac{e^2\omega^2}{6\pi\varepsilon_0 mc^3} \tag{7}$$

So now we can plug $\mathbf{x} = \mathbf{x}_0 e^{-i\omega t}$ in to our equation here,

$$\begin{aligned} \mathbf{x} &= \frac{e}{m}\frac{1}{\omega_0^2 - \omega^2 - i\omega\gamma}\mathbf{E}_0 e^{-i\omega t} \\ &= \frac{e}{m}\frac{1}{\sqrt{(\omega_0^2-\omega^2)^2 + \omega^2\gamma^2}}\mathbf{E}_0 e^{-i(\omega t-\delta)} \\ &\quad \tan\delta = \frac{\omega\gamma}{\omega_0^2 - \omega^2} \end{aligned}$$

#220257 - $15.00 USD Received 1 Aug 2014; revised 7 Sep 2014; accepted 8 Sep 2014; published 22 Sep 2014

Therefore, scattering wave field intensity can be obtained as following:

$$E = \frac{e\ddot{x}}{4\pi\varepsilon_0 c^2 r}\sin\alpha \tag{8}$$

where, α is the angle between the incident wave field $\mathbf{E}_0$ and scattering direction, so the average scattering energy flow

$$\bar{S} = \frac{e^4 E_0^2}{32\pi^2\varepsilon_0 c^3 m^2 r^2}\frac{\omega^4}{(\omega_0^2-\omega^2)^2+\omega^2\gamma^2}\sin^2\alpha \tag{9}$$

the scattering power derived from the surface integral as

$$P = \frac{8\pi}{3}r_e^2\frac{\omega^4}{(\omega_0^2-\omega^2)^2+\omega^2\gamma^2}I_0^2. \tag{10}$$

The scattering cross section could be obtained

$$\sigma = \frac{8\pi}{3}r_e^2\frac{\omega^4}{(\omega_0^2-\omega^2)^2+\omega^2\gamma^2} \tag{11}$$

The resonance effect could be acquired once $\omega = \omega_0$, along with $\omega_0 \gg \gamma$. Therefore, once the graphene surface plasmonic wave excited, the resonance scattering cross section would be only confined around the interface between ZnO microrod and graphene monolayer on the subwavelength scales.

2.4. Whispering gallery mode lasing characteristics enhancement derived from hybridized plamonic whispering gallery mode microcavity

In order to testify that graphene monolayer coated ZnO hexagonal microrod could provide a platform to realize the coupling interaction between surface plasmonic mode with conventional WGM mode, the hybridized plasmonic WGM microcavity demonstrated in Fig. 3 were prepared experimentally. In the experiment, the light spot area of pumped light source is well maintained. Excitation energy will be used as energy pump parameters. Take the bare ZnO hexagonal microrod (BMC) for example, once the excitation power is further increased to 20 μW, more peaks appear at 392.07848 nm, 392.44102 nm, 392.79636 nm and 393.18337 nm with the full width at the half maximum (FWHM) $\delta\lambda \sim 0.08105$ nm, and the peak intensity increases more dramatically. The significant nonlinear response of the output power to the peak pump intensity shown in Fig. 5(c) indicates a transition from spontaneous emission to stimulated emission. The multipeak spectral structures reveal multiple lasing modes with the average mode spacing $\Delta\lambda$ of 1.0 nm. It is estimated that the Q-factor of this microcavity is about 5000 according to the equation, $Q = \lambda/\delta\lambda$, where λ and $\delta\lambda$ are the peak wavelength and FWHM, respectively. The emission intensity increases slowly when the excitation power density is below 5 μW, and it increases rapidly when the excitation power density is larger than 5 μW. This indicates the lasing threshold is at about 5 μW. Therefore, ZnO hexagonal microrod can be used to realize the WGM lasing. It clearly confirmed the WGM lasing mode characteristics.

Compared with the bare ZnO microrod, two kinds of hybridized plasmonic WGM microcavities were built, they are ZnO microrod placed on SiO_2 substrate coated by graphene monolayer on the upper surface of microrod (GMC1), and ZnO microrod placed on SiO_2 substrate coated by two graphene monolayers on the upper and down surface of microrod respectively (GMC2). Corresponding dazzling blue-violet light emitted from the ZnO microrod, the lasing intensities and lasing threshold results from a bare ZnO hexagonal microrod, graphene monolayer coated

#220257 - $15.00 USD Received 1 Aug 2014; revised 7 Sep 2014; accepted 8 Sep 2014; published 22 Sep 2014

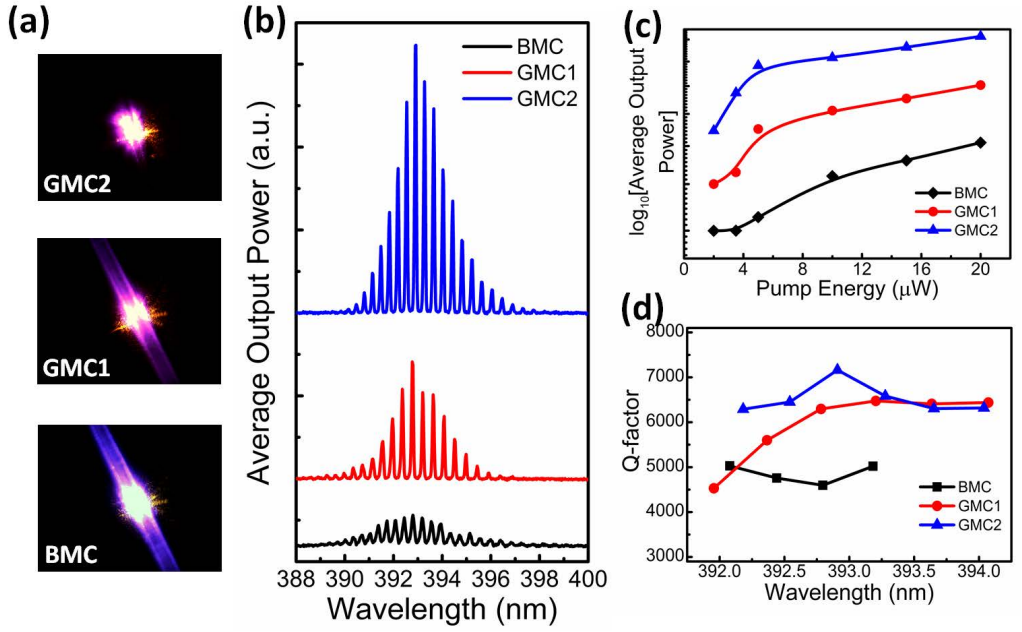

Fig. 5. (a) demonstrate the far-field image of the lasing a bare ZnO hexagonal microrod cavity (BMC), ZnO microrod coated by a graphene monolayer (GMC1), and ZnO microrod coated by two graphene monolayers by means of the upper and down surface of ZnO hexagonal microrod (GMC2), taken by a digital camera, respectively; (b) demonstrate emission spectra of a bare ZnO microrod, intensity modulation of ZnO microrod coated by a graphene monolayer, and intensity modulation of ZnO microrod coated by two graphene monolayers optically pumped with 20 μW, respectively; (c) reveals the nonlinear response of the output power to the peak pump intensity; (d) reveals the calculated Q-factors of WGM microcavities for a bare ZnO hexagonal microrod cavity, graphene monolayer coated ZnO hexagonal microrod cavity, and graphene monolayers coated the upper and down surfaces of ZnO hexagonal microrod cavity, respectively.

ZnO hexagonal microrods were shown in Fig. 5. Figure 5(b) indicates the emission spectra with corresponding excitation power 20 μW. Figure 5(a) illustrates that optical field confinement can be improved obviously. The improvement could reduce the waveguide loss of ZnO hexagonal microrod microcavity, significantly. It is well known that, graphene plasmon can be used able to form the hybrid spaser, that could provide a platform to realize the surface plasmon amplification [32,37,38,48]. Meanwhile, this amplification can be used to support the surface plasmon excitations with an optical field strongly localized near the graphene monolayer. The confinement of optical field could induce more photons imprisoned within the WGM cavity, thus avoid the escape from the conventional optical WGM microcavity. When the contact facets between graphene monolayer with ZnO hexagonal microrod increase, the confinement of the localized fields will be more obvious, as well as the enhancement of the lasing intensities. In the case of the improved lasing intensity, the corresponding threshold of the laser decreases followed shown in Fig. 5(c) from 5 μW to 2 μW. This makes the light more difficult to escape or couple to free space due to the graphene monolayer. Metallic nanostructures often demonstrate surface plasmon resonances confined at the interface, which are characterized by strongly enhanced near-fields produced by charges stopping at the surface of the metal. Because of interaction of light with graphene determined by the local electromagnetic fields (induced on the graphene

#220257 - $15.00 USD Received 1 Aug 2014; revised 7 Sep 2014; accepted 8 Sep 2014; published 22 Sep 2014

monolayer), this coupling interaction can effectively be increased by placing excitons source of ZnO microrod close to the graphene. According to Figs. 5(a) and 5(b), when increasing the pumping energy, strong absorption of ZnO microrod would lead to more coherent photons generated by means of transferring the energy from graphene monolayer. The operation of lasing requires ZnO microrod whose excitation energy can be transferred nonradiatively to a coupled hybridized plasmonic WGM resonator, increasing the amplitude of the surface plasmonic mode, which could result in the enhancing total internal reflection of WGM optical microcavity. It can be found that in a hybridized plasmonic WGM resonator, graphene monolayer can indeed lead to the enhancement of the total internal reflection, whilst accompanied with lower lasing threshold.

In general, methods can be used to improve the Q-factors of conventional optical microcavity, such as local field adjustment, radiation energy recycling, and the modes matching methods. According to the results of theoretical studies, it can be found that graphene monolayer coated ZnO microrod could compensate the energy loss of photons at the mirror surface, which can enhance local field distribution at the interface, as well as the enhancement of radiation energy recycling. On the basis of Fig. 5(a), graphene monolayers have compensated the mirror loss and waveguide loss effectively. Consequently, to complete the characterization of hybridized plasmonic WGM microcavities, the Q-factor of the resonance observed were investigated. To estimate the improvement of graphene on the performance of WGM lasing characteristics, Q-factor of the microcavity were calculated according to the experimental results. Details of the calculated results can be referred to Fig. 5(d) due to the definition of $Q = \lambda / \delta\lambda$. These values are higher than the previously reported value of 1500 for WGM lasing of a 4 μm diameter ZnO microdisk grown on a Si-masked SiO_2 substrate [2, 5]. According to Fig. 5(d), Q-factor of ZnO hexagonal microrods have improved obviously due to graphene monolayer, that the Q factors of the hybridized plasmonic WGM microcavities are generally higher 2000 than a bare ZnO microcavity. Compared with silver film coated optical microcavity, higher-Q factors enhancement have been realized through graphene monolayer coated ZnO hexagonal microrod along with the lower ohmic losses of graphene than silver [3, 21, 40]. Therefore, graphene monolayer can indeed lead to the enhancement of higher Q factor, and narrower line width and so on.

For the past few years, it has been many reports related though general topics such as WGM resonators and surface plasmons by studying, modeling and simulating, there is still little relevant reports of quantitative relationship and three-dimensional dynamic simulation [47,55–57]. More attention on the experiment has been focused on by J. T. Li *etal*., and has demonstrated the optical field confinement and lasing enhancement in ZnO WGM microcavity [47]. Immediately following the related topics, theoretical research and the corresponding dynamic problems on fundamental physics under the graphene plasmon in the UV wavelength region and UV lasing were taken into account in the paper. The focus of our research is more looking forward to find a new approach to enhance, or improve the performance of devices based on the conventional microcavity. This is within the application of study on the surface plasmon and micro-nano structure, however, beyond it, the duo are capable of magic, such as beyond the diffraction limit, more is to achieve a new type of optical cavity structures [55–57], such as spaser [32, 37, 38, 48], plasmonic optical cavity (this kind of novel cavities derived from the diffraction limit, nanostructures, and the Q is subject to the metallic loss) [3, 11, 20, 21, 55, 57], and nanolaser [7, 22, 24, 56]. From a more fundamental point of view, the simulations performed for a bare ZnO hexagonal microrod and hybridized plasmonic WGM microcavities derived from graphene monolayers coated ZnO hexagonal microrod illustrate that the field decays exponentially into ZnO microrods from the surface, yields the hybridized surface plasmonic modes composed of the surface plasmonic modes and conventional cavity modes, as well as

#220257 - $15.00 USD Received 1 Aug 2014; revised 7 Sep 2014; accepted 8 Sep 2014; published 22 Sep 2014

the modulation of the localized field distribution along the mirror surface of microcavity. With the help of graphene monolayer, ZnO hexagonal microrod can form a new kind of plasmonic resonant cavity. The hybridized plasmonic WGM microcavities have been present by adopting graphene monolayer enhancing the internal reflection within the conventional WGM microcavities to mitigate the radiation loss, mirror and waveguide loss, while using hybrid graphene monolayer-air-ZnO hexagonal microrod for strong confinement. Higher-Q, approaching 7000, along with strong optical field mode confinement, can lead to the enhancement of spontaneous emission rate by up to 10-folds. Based on the theoretical and experimental results, it can be found that graphene does bring substantial improvement of the WGM lasing characteristics, such as the modulation and improvement of optical field confinement, high-Q factors, and lasing intensities.

3. Conclusion

High-Q hybridized plasmonic WGM microcavities were proposed, and the relevant hybridized plasmonic microcavity dynamics were also explored. ZnO hexagonal microrods served as the adequate gain materials as well as a intrinsic optical WGM microcavities. Distinctive effect on renormalized saddle point resonance at 4.64 eV of graphene π-plasmon can open the door for a wide range of applications in the UV region. Compared with a bare microrod, prominent optical field confinement and lasing enhancement can be observed from the hybridized surface plasmonic WGM microcavities, especially for the up and down surfaces of microrod covered by graphene monolayers. The apparent improvement the optical field confinement can be derived from the strongly localization of local plasmonic field at the graphene surface. The evanescent wave field excited along the interface between ZnO/graphene provides a platform to achieve the coupling interaction between graphene plasmonic modes with conventional microcavity modes in hybridized plasmonic WGM microcavities. Meanwhile, this kind of coupling can improve the feedback, which lead to the improvement of WGM lasing characteristics. This remarkable improvement can bring two benefits: graphene surface plasmons can be applied to wide bandgap semiconductor devices in the UV region, and high-Q plasmonic microresonators can be obtained on the basis of graphene monolayers. Thus the present system has great advantages over a single microcavity or graphene, and holds great potential in quantum optics, nonlinear optics and highly sensitive biosening.

Acknowledgments

We thank Pro.Yong-Qiang Ning for providing *COMSOL Multiphysics* software friendly for this work. This work is supported by National Basic Research Program of China (973 Program) under Grant Nos. (2011CB302002, 2011CB302004), the Key Program of the National Natural Science Foundation of China (11134009), the National Natural Science Foundation of China under Grant Nos. (11404328, 21101146, 61177040), the 100 Talents Program of the Chinese Academy of Sciences.

#220257 - $15.00 USD Received 1 Aug 2014; revised 7 Sep 2014; accepted 8 Sep 2014; published 22 Sep 2014